ACS OMEGA

Open Access

http://pubs.acs.org/journal/acsodf

Article

Research on Oil and Gas Adsorption Optimization Based on CFD Modeling and Process Simulation

Bin Liu, Mengjiao Zhang, Ye Tao, Zhe Cui, and Wende Tian*

Cite This: *ACS Omega* 2024, 9, 29805−29819

Read Online

ACCESS | Metrics & More | Article Recommendations

ABSTRACT: In the process of oil extraction and refining, some of the liquid light hydrocarbon components will inevitably evaporate into the atmosphere, causing serious air pollution and safety hazards. This paper is focused on oil and gas adsorption systems to comprehensively optimize key parameters by combining computational fluid dynamics (CFD) modeling with process simulation, enabling the efficient treatment of hazardous materials. First, a CFD model of the hydrocarbon adsorption process is established to the porous media model by a user-defined function (UDF). Subsequently, the mass transfer process of oil and gas in porous media is successfully simulated to obtain the gas distribution in an industrial fixed bed adsorption tower. The adsorption tank is intensified, and the gas distribution in the tank is improved by optimizing the height-to-diameter ratio of the equipment and the design of the intake distributor. Third, the cyclic two-tank adsorption model of the pressure swing adsorption (PSA) process is established for key parameters optimization. Finally, the operating parameters and conditions of the PSA process are suspected by considering five factors affecting the adsorption efficiency: adsorption time, adsorption pressure, adsorption temperature, feed flow rate, and purge ratio of the washing step.

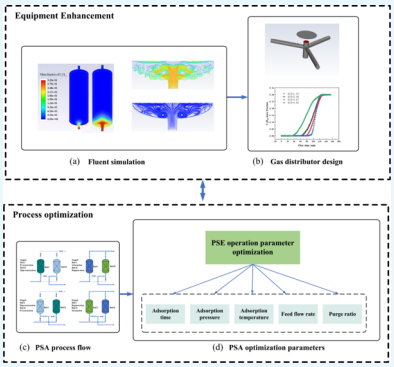

1. INTRODUCTION

In the petrochemical industry, a plethora of highly volatile light hydrocarbon compounds are found within the composition of crude oil. These compounds, often referred to as volatile organic compounds (VOCs), represent a diverse group of substances in which volatile light hydrocarbons are one of prominent constituents. In the process of their extraction, refining, storage, transportation, and application, some of the liquid light hydrocarbon components will inevitably evaporate and escape into the atmosphere due to the limitations of technology, process, and equipment conditions. This will not only cause serious oil loss, resulting in energy waste and economic loss, but also cause environmental pollution, endanger human health, and bring many safety problems to enterprises.[1] Many VOCs have been found to cause photochemical smog and haze in cities, posing health risks to humans, such as feeling irritated, causing severe respiratory or metabolic disorders, and even carcinogenic effects.[2] Globally, VOCs emissions from industrial sources accounted for 46.55% of anthropogenic VOCs releases, and stationary combustion accounted for 3.2%.[3] Hence, it becomes imperative to implement VOCs recycling as a crucial step toward enhancing energy efficiency, mitigating economic losses, safeguarding the ecological environment, and eliminating potential safety hazards. In recent decades, there has been a proliferation of technologies designed to mitigate oil and gas, ranging from thermal oxidation and absorption to adsorption and catalytic oxidation. However, these methods frequently give rise to secondary pollution and the release of additional contaminants like halides, NO_2, SO_2, and other byproducts.[4] Furthermore, the utilization of absorption technology in the oil and gas treatment is often hampered by its high costs and the complexity involved in selecting suitable solvents.[5] In contrast, adsorption has emerged as a particularly promising alternative. Currently, adsorption stands out as a mature, energy-efficient, and environmentally friendly method for oil and gas recovery.[6] Compared to alternative separation techniques, adsorption typically demands lower energy consumption, boasts broader application possibilities, achieves higher removal efficiency, generates less secondary pollution, and excels in the treatment of polluted gases characterized by low concentrations and high air volumes.[7]

In practical industrial applications, the oil and gas adsorption processes usually take place in a fixed adsorption bed. Traditional experimental research methods are often limited by the equipment itself and external resource conditions. Although theoretical research methods do not have these disadvantages, their analysis process is complex and requires simplification of the calculation pair. Moreover, in nonlinear

Received: April 11, 2024
Revised: May 25, 2024
Accepted: June 13, 2024
Published: June 26, 2024

https://doi.org/10.1021/acsomega.4c03136
ACS Omega 2024, 9, 29805−29819

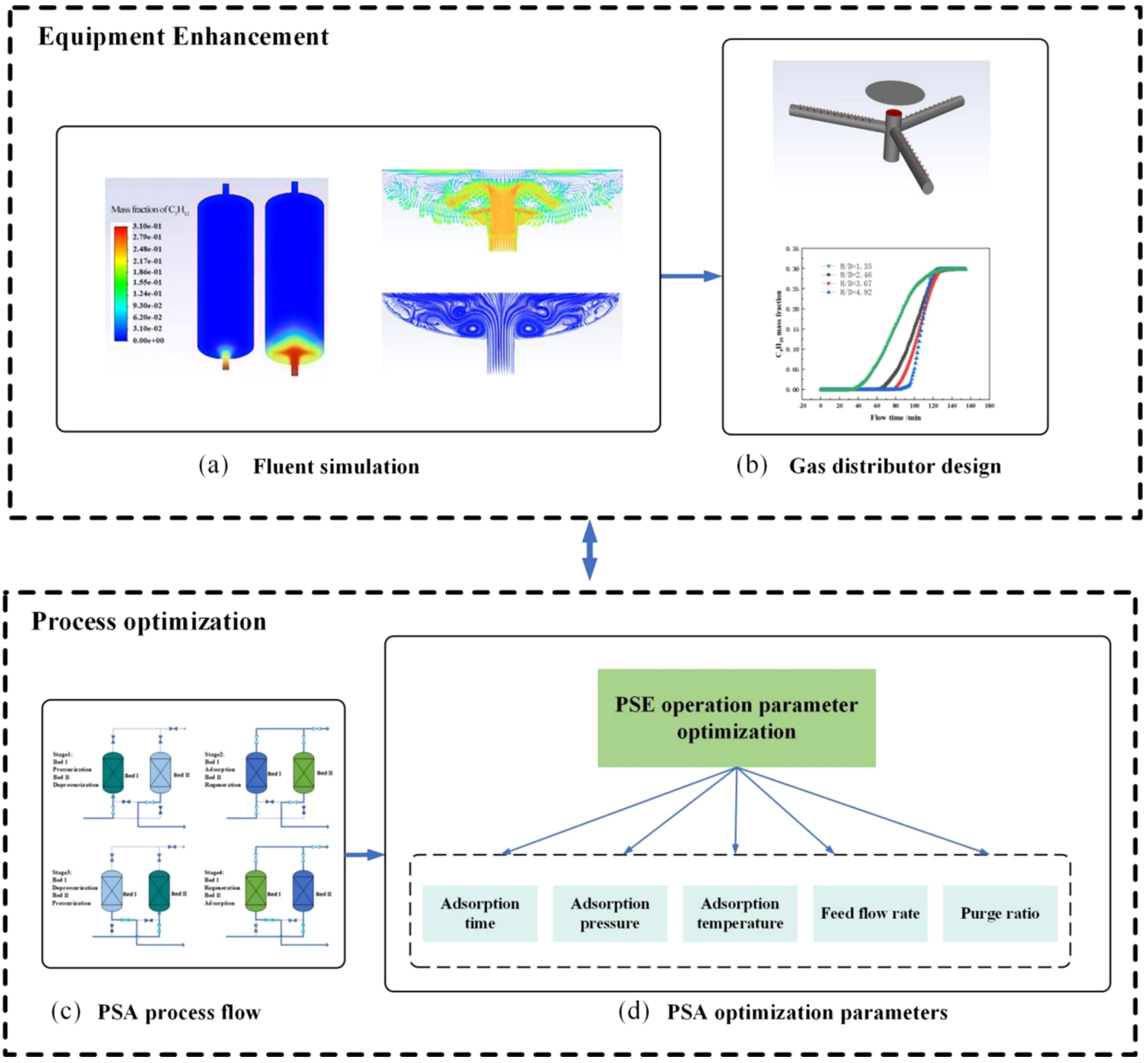

Figure 1. Overall structure of the proposal.

situations, only a few flows can be accurately calculated based on the analysis results. Numerical simulation of adsorption processes is therefore essential to effectively improving process design. Computational fluid dynamics (CFD) simulation is a reliable simulation technique. The CFD simulation method overcomes the shortcomings of experimental and theoretical methods, so it can be used to simulate fluid flow and component transport in dynamic adsorption processes, thereby optimizing equipment and operating conditions.[8] The basis and paramount importance of performing CFD simulations are to develop suitable and effective mathematical models for different flow processes. In most of the works, the mathematical models are based on the finite element method (finite difference or finite volume) derived from the mass and energy balance equations for a 1D piston flow. The feasibility of the piston flow assumption has been widely accepted due to the relatively slow flow of gases through porous beds. With the advancement of CFD technology, the porous media model built into CFD solvers has been used for the simulation of sorbent beds, but it can only handle flow problems, and for gas mass transfer processes within the sorbent, the addition of source terms through user define function (UDF) is required. Di Carlo et al.[9] developed CFD mathematical models for the simulation of stationary adsorption beds, where the "Brinkman Forchheimer" model is used for porous media simulation and the Ergun equation is used for pressure drop calculations. Freundlich isotherm and linear driving force (LDF) models were integrated for adsorption kinetics. But it is not specified how the models were integrated with each other. Chen et al.[10] coupled CGMD and CFD-PBM simulations using the transport equations of surfactants at the bulk and interface. Compared with traditional CFD-PBM simulations, the coupled model can greatly improve the simulation of DSD, Sauter mean diameter, median diameter, and span for highly dispersed phase quantities (DPA). Salim Bded[11] investigated the effect of viscosity changes on natural convection in a confined space and predicted the flow field and

https://doi.org/10.1021/acsomega.4c03136
ACS Omega 2024, 9, 29805−29819

heat transfer in a bilayer porous medium using the Darcy model in a commercial CFD package, but did not simulate or analyze the concentration field. Bai et al.[12] simulated the fixed bed adiabatic adsorption/desorption process and calculated the heat and mass transfer rates using the LDF model. Francesco Montecchio et al.[13] developed a CFD model that combines UV radiation, reaction kinetics, and fluid dynamics. This model describes the behavior of laboratory-scale UV reactors and concludes that the developed CFD model will become an important tool for reactor amplification. Nouh et al.[14] simulated the packing properties and pressure drop using the built-in porous media model in ANSYS Fluent and wrote a UDF code that introduces the component transport phenomena of the gas between the bulk term and the adsorbent using a mass source term. The LDF model, which describes the kinetics of adsorption, is combined with a porous media model. The heat change associated with the adsorption process is introduced with an energy source term, thus simulating the flow state and heat exchange process of the gas in the porous medium in an approximately realistic way. Hou et al.[15] developed a computational area model for a steam recovery carbon canister and numerically simulated the internal structure of the canister using CFD. The one-dimensional hydrodynamic model, introduced by Gomes et al., has been integrated with the adsorption process and subsequently validated.[16] Hou et al.[17] developed a nonconstant three-dimensional mathematical model of adsorbed benzene and investigated the effects of inlet benzene concentration and gas velocity on the outlet benzene concentration, temperature, and pressure distribution in the U-tube. Buzanowski et al.[18] confirmed that the pressure drop leads to a broadening of the trailing penetration curve, which is detrimental to the adsorption process, and their simulations agreed well with the results of the adsorption and desorption experiments. Darakchiev et al.[19] found that with the development of large adsorption towers, the uniformity of gas distribution has become an important factor limiting the operating efficiency of the adsorption tower. Waldron's research has shown that uneven gas distribution can lead to poor adsorption efficiency and shorten bed penetration time.[20] A distributor with excellent performance not only effectively provides uniform predistribution of the gas before it flows into the packed bed but also prevents the direct effect of high-velocity gas on the adsorption bed. In general, industrial gas distributors including porous plate distributors,[21] circular distributors,[22] fractal distributors,[23] spherical microporous gas distributors,[24] etc. are indispensable.

The main structure of the remaining part is shown in Figure 1. First, the mesoscopic oil and gas adsorption system is modeled by CFD simulation. Based on the primary model, the height-to-diameter ratio (H/D) and inlet gas distribution are optimized depending on mass transfer, momentum transfer, and reaction mechanisms to achieve the enhancement of the equipment. After the above optimized mesoscopic parameters were obtained, the dynamic macroscopic oil and gas adsorption system is established and further optimized. Finally, the performance of the optimized oil-gas adsorption process based on both mesoscopic and macroscopic levels is investigated to verify the reliability of the optimization results.

In this paper, a 3D model of the oil and gas adsorption tank with activated carbon as the adsorbent is established using CFD simulation soft, and the distribution state of oil and gas in the adsorption tank is studied. Equipment enhancement is carried out by optimizing the height-to-diameter ratio of the adsorption tank and adding an inlet gas distribution device to improve the oil and gas adsorption efficiency. Then, a complete four-step variable pressure adsorption model is established using Aspen Adsorption, and a dynamic simulation of the whole process of adsorption and desorption is carried out. The proposed method will improve resource utilization efficiency while efficiently treating hazardous pollutants in oil and gas and provide reference for other oil and gas systems with similar pollutants.

2. MODEL DESCRIPTION

2.1. Adsorption Tank Model. The physical model is based on the actual oil and gas adsorption tank equipment in industry, and the activated carbon bed is fixed using wire mesh. During gas adsorption and desorption, the adsorbent particle position is fixed, while the oil and gas flow in the activated carbon particle gap and mass transfer take place between the gas phase and the activated carbon adsorption phase, which belongs to the fixed bed adsorption model. Fixed bed reactors have received a lot of attention as catalytic devices and adsorption equipment commonly used in the chemical industry, which are generally divided into vertical and horizontal types. Of these, the vertical fixed bed reactor is the most commonly used one; therefore, the fixed bed form is used in this paper. Figure 2 shows a schematic diagram of the geometry of an oil and gas adsorption tank.

Figure 2. Geometry of the fixed bed adsorption tank.

https://doi.org/10.1021/acsomega.4c03136
ACS Omega 2024, 9, 29805−29819

In the adsorption step, the oil and gas enter through the bottom inlet and exit from the top. The materials used in the simulation are air, gas-phase butane, and pentane, and the actual gas air, gas-phase butane, and pentane properties are imported from the FLUENT database. A mathematical model is developed for the oil and gas sorption process and coupled to the porous media model built into the Fluent solver via UDF to simulate the flow and sorption mass transfer processes of the oil and gas mixture in the porous zone. The filled layer of the porous medium is considered as a continuous medium, and the results are analyzed using a numerical model that solves the nonconstant continuum momentum and mass equations, which allows the spatial distribution of the adsorbed quantities to be simulated. The main advantage of using CFD to simulate the adsorption process is that the distribution of velocity fields, concentration fields, etc. can be obtained at any time and at any position. This clearly exposes the limitations of the analytical solution, which can account for only the steady state situation. In contrast, computational fluid dynamics also accurately accounts for the entire transient state before a steady state level is reached. A graphical representation of the mass fraction of butane simulated by CFD is given in Figure 3. Due to adsorption, dramatic changes in butane concentration can be clearly observed as the gas moves along the adsorption bed.

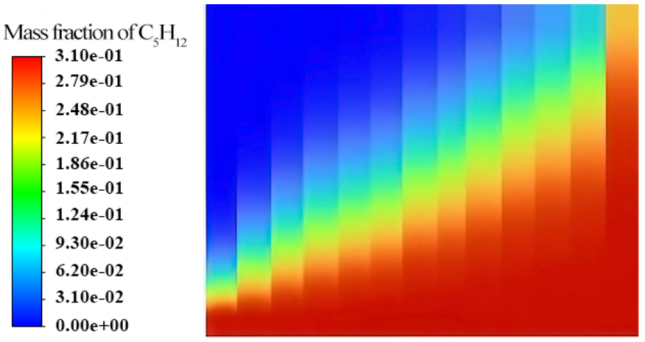

Figure 3. Sketch of the concentration distributions of oil and gas components at different moments.

2.2. Meshing. Due to the relatively simple geometry of the tank, a quadrilateral cell mesh is considered for fine meshing, and an expansion layer is added to the walls to encrypt the local mesh. A mesh sensitivity study is carried out to determine the appropriate mesh size, taking into account the calculation time and accuracy of the results. The smaller the time-step size, the more accurate the calculation, but the larger the computational resources required. We evaluated the number of grids for four specifications (initial coarse grid 20640, medium grid 50374, fine grid 100079, and very fine grid 150924) and four time-step-sizes (initial time step: 0.01 s, medium time step: 0.005 s, and very fine grid 150924); step: 0.01 s (medium time step: 0.005 s, fine time step: 0.002 s, and very fine time step: 0.001 s). The grid size of 100079 is finally chosen as shown in Figure 4. According to the grid quality evaluation report, it does have a higher quality than the grid size of 50374 without making the calculation time too long. The maximum cell size is 2.16 mm. The simulation area is divided into 100079 cells and 101036 nodes. The following grid qualities are reported by FLUENT: the minimum orthogonal quality is 0.8571 and the average orthogonal quality is 0.99932, where the orthogonal quality ranges from 0 to 1, with values close to 0 corresponding to low quality. The average cell

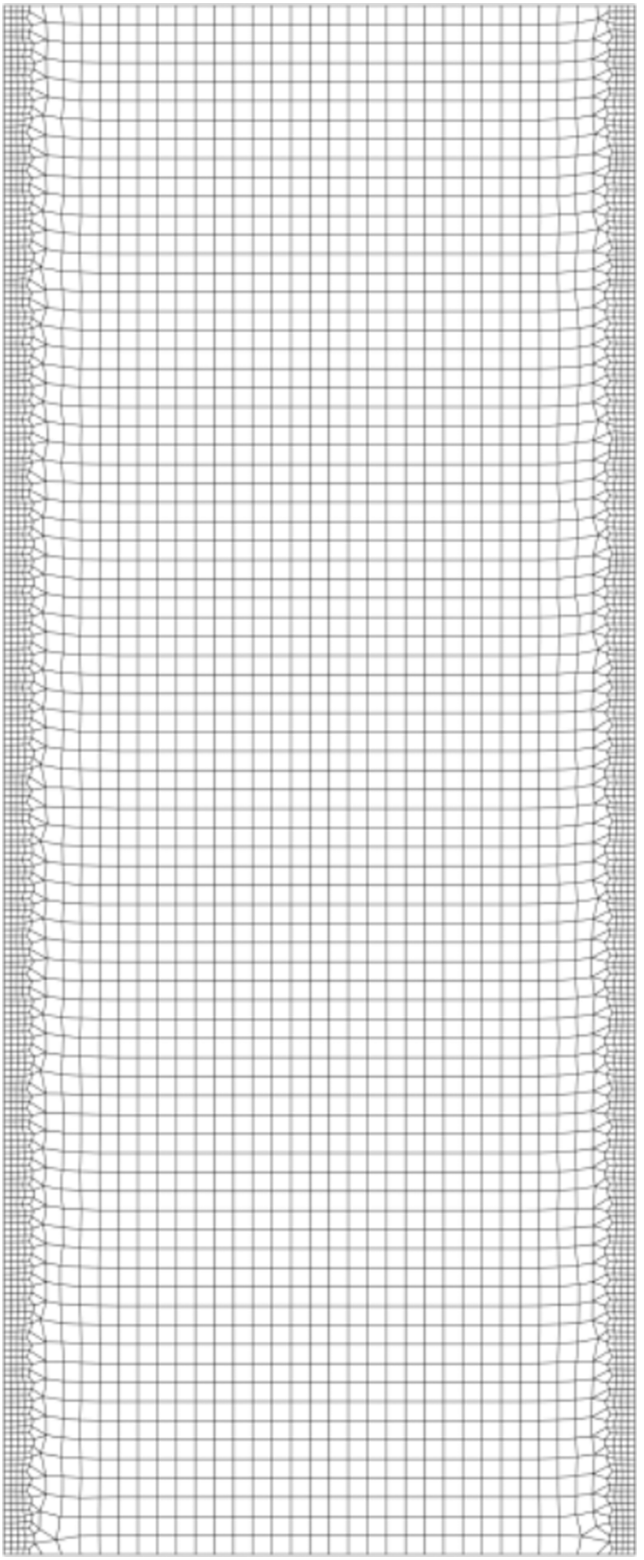

Figure 4. Quadrilateral grids with 100079.

mass is 0.99337, and the minimum cell mass is 0.76254, where the cell mass ranges from 0 to 1. A value of 0 indicates the closest to the ideal state with a better mesh quality, and the quality test results show that the mesh quality meets the accuracy requirements needed for the calculation.

The meshed model is imported into the CFD solver for transient solving. Constant flow is chosen for the pressure-based

https://doi.org/10.1021/acsomega.4c03136
ACS Omega 2024, 9, 29805−29819

Table 1. CFD Solver Settings

parameters	settings	notes
solvers	pressure-based solvers	constant flow
physical model	inlet turbulence models	k-ε model
	porous media models	laminar flow
boundary conditions	velocity inlet	
	pressure outlet	outlet to atmosphere
	slip-free wall surfaces	fluid in contact with housing
	porous leapfrog surface	fluid in and out of porous media surface
method of solution	coupled algorithms	pseudo Transient Status
momentum discretization scheme	second order windward	
energy discretization scheme	second order windward	
pressure interpolation format	second order windward	
density interpolation format	second order windward	Ideal gas law
time term discrete format	first-order implicit windward	
discretization Scheme	standard discrete	pressure solving
subloose factor	default values	
gravitational force	g = 9.8 m/s^2	
monitoring residuals	<0.001	
initial condition setting	standard initialization	based on entrance coordinates

solvers. The k-ε model is chosen as the inlet turbulence model, and the laminar flow is used as the porous media models. The velocity inlet and pressure outlet boundary conditions are used. For the wall surface, which is an adiabatic wall, the no velocity slip and no mass penetration conditions are used. The standard wall function method is used to compensate for the wall boundary layer effect. The Coupled algorithm is selected as the Pseudo Transient Status. The Second Order Windward is chosen for the Momentum Discretization Scheme, Energy Discretization Scheme, pressure interpolation format, and density interpolation format. First-order implicit windward is chosen as the time term discrete format. The discretization Scheme is chosen as Standard Discrete. The subloose factor is the default value. Gravity g = 9.8 m/s^2, monitoring residuals < 0.001, initial condition setting to standard initialization based on entrance coordinates. The detailed settings of the solver are listed in Table 1.

CFD simulation boundary arrangement is shown in Figure 5. Slip-free wall surfaces are selected in CFD, the gas velocity is 0.45 m/s, the pressure at the outlet is atmospheric, and the walls are adiabatic.

2.3. Model Assumptions. The simultaneous occurrence of momentum, heat, and mass transfer in the adsorption bed makes the process more complex. In order to reduce the complexity of CFD simulations and establish an effective mathematical model, the actual adsorption process must be simplified with the following assumptions:

- The oil and gas mixture is approximated as an ideal gas and its physical properties can be estimated by the mixing law.
- The solid adsorbent only adsorbs the oil and gas and does not act on the other components. Although the adsorbent material does adsorb a small proportion of the other components, this is negligible compared to the oil and gas.
- The oil and gas contains only the major gas components, that is, C_4H_{10}, C_5H_{12}, and air, and does not include the minor components.
- In the porous filled bed zone, the adsorbent particles are uniformly distributed.
- The external mass transfer resistance is zero, that is, the concentration of oil and gas in the volumetric flow is the same as the concentration of oil and gas on the outer surface of the adsorbent.
- The tank is adiabatic and there is a local thermal equilibrium between the gas and the adsorbent.

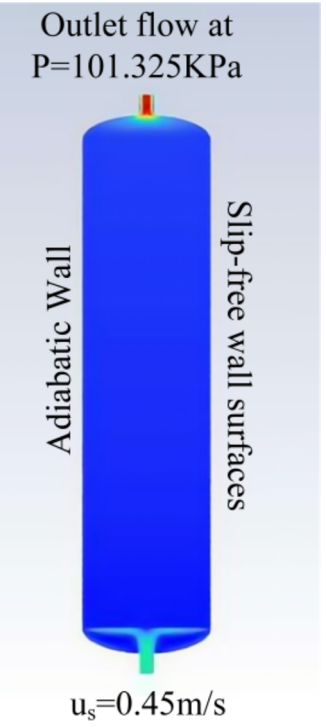

Figure 5. Boundary configuration diagram in the CFD.

2.4. Numerical Solution Methods. The simulation model is based on the equations of conservation of momentum, mass, and energy, so the model equations given by a set of partial differential algebraic equations are more difficult to solve. When the axial diffusion of the gas stream is not significant, the concentration profile may be steeper, and such profiles require a refined grid for processing with a large amount of computational effort. It is therefore particularly critical to reduce the computational effort when optimizing the sorption process; therefore, the values should be discretized. In this article, the

https://doi.org/10.1021/acsomega.4c03136
ACS Omega 2024, 9, 29805−29819

computational domain is discretized using the finite difference method, which converts a set of partial differential algebraic equations into a set of differential algebraic equations. In the solution process of this paper, the numerical solution method is chosen as the more stable windward difference method, which has a shorter simulation time; the simulation results are reasonably accurate, and the accuracy can be improved by increasing the number of nodes. As the porous media area is an all quadrilateral grid, in which the flow direction is the same as the grid direction, the spatial discretization method can meet the calculation accuracy requirements by choosing the first-order windward discretization format. This section describes the general fluid dynamics control equations modified for the porous media model. The simulation model, rooted in the principles of momentum, mass, and energy conservation, is underpinned by a complex set of partial differential algebraic equations for its model equations, rendering them notably more complex to resolve. In cases where the axial diffusion within the gas stream remains negligible, the resultant concentration profiles tend to exhibit steeper gradients, necessitating the adoption of a meticulously refined grid for computational processing—an endeavor that demands a substantial computational outlay. Therefore, it is of paramount importance to curtail the computational burden during the optimization of the sorption process, prompting the need for value discretization. In this study, we discretize the computational domain through the finite difference method, a transformation that transmutes a collection of partial differential algebraic equations into a suite of differential algebraic equations. Within the framework of this paper's solution methodology, we opt for the more stable windward difference method as the numerical solver, noted for its reduced simulation time and reasonably accurate results. Enhanced precision can be achieved by augmenting the number of computational nodes. Given that the porous media region exclusively employs a quadrilateral grid configuration and aligns its flow direction with the grid orientation, the spatial discretization method effectively fulfills the stipulated accuracy requirements through the selection of the first-order windward discretization format. This section elaborates upon the adaptation of general fluid dynamics control equations to accommodate the porous media model's unique characteristics.

2.4.1. Mass Balance Equation. The adsorption separation process is a process in which mass transfer phenomena occur between the gas component and the solid adsorbent. The adsorbed gas component accumulates on the surface of the porous medium, which can be expressed as a loss of the gas component, resulting in a reduction in the mass of the gas in the bulk phase, which is handled by adding a negative mass source term to the mass equation, and the gas component in the process satisfies the mass balance equation. The mass continuity equation for unsteady flow within a porous medium can be expressed as shown in eq 1.

$$\frac{\partial \varepsilon \rho_f}{\partial t} + \nabla(\varepsilon \rho_f \vec{v}) = S_m \tag{1}$$

where

ε is the porosity of the fixed bed

ρ_f is gas density, kg/m^3

t is time, s

$\vec{v}$ is the physical velocity vector, m/s

S_m is the mass source term due to chemical reactions or other mass sources, e.g., gas adsorption or desorption, as shown in eq 2. R_i is the production rate of species i due to reactions, and S_i is the rate of adsorption/desorption of species i.

$$S_m = \sum (R_i + S_i) \tag{2}$$

In order to predict the local mass fraction Y_i of each substance, a substance transport equation based on the convective diffusion of the substance is used. The first term on the left-hand side of the equal sign of eqs 3 and 4 is the change in concentration of substance, the second term is the convective term, and the third term is the diffusion term. The right-hand side of the equal sign is the mass source term.

$$\frac{\partial(\varepsilon \rho_f Y_i)}{\partial t} + \nabla(\varepsilon \rho_f \vec{v} Y_i) - \nabla\left(\varepsilon \rho_f D_{i,m} \nabla Y_i + \varepsilon D_{T,i} \frac{\nabla T}{T}\right) = -S_i \tag{3}$$

$$S_i = R_i - \mathrm{MW}_i \rho_b \frac{\partial q_i}{\partial t} \tag{4}$$

where

Y_i is the mass fraction of species i

$D_{m,i}$ is the mass diffusion coefficient for species i in the mixture, m^2/s

$D_{T,i}$ is the thermal diffusion coefficient, m^2/s

S_i is the source term of species i

R_i is the source term of species i due to reactions

MW_i is the molar mass of species i, kg/kmol

ρ_b is the density of the bed, kg/m^3

ε is the porosity of the bed

q_i is the amount of adsorption of species i, kmol/kg.

2.4.2. Momentum Balance Equations. For all flow problems, the CFD simulation solves the mass balance equation and the momentum balance equation by default. For flow problems in porous media, where the fluid is additionally subjected to resistance from the pores of the porous media, a momentum source term needs to be superimposed on the default momentum eq 5 to describe the relationship between flow velocity and pressure drop.

$$\frac{\partial(\varepsilon \rho_f \vec{v})}{\partial t} + \nabla(\varepsilon \rho_f \vec{v}\vec{v}) = -\varepsilon \nabla p + \nabla(\varepsilon_i \bar{\bar{\tau}}) + \varepsilon \rho_f \vec{g} + \vec{S} \tag{5}$$

where

p is the static pressure, pa

$\bar{\bar{\tau}}$ is the stress tensor, pa

$\rho \vec{g}$ is the gravitational body force, kg/m^2/s^2

$\vec{S}$ is the momentum source term, consisting of a viscous loss term (the first term on the right-hand side) and inertial loss term (the second term on the right-hand side), as shown in eq 6. The viscous loss constant D_{ij} quantitatively describes the viscous loss caused by fluid flow in porous media, and the inertial constant C_{ij} provides a correction for the inertial loss in porous media. This constant can be seen as the loss coefficient per unit length along the direction of flow.

$$\vec{S} = -\left(\sum_{j=1}^{3} D_{ij} u v_j + \sum_{j=1}^{3} C_{ij} \frac{1}{2} \rho |v| v_j\right) \tag{6}$$

where

u is the viscosity, m^2/s

ρ is the density, kg/m^3

v is the velocity, m/s

https://doi.org/10.1021/acsomega.4c03136
ACS Omega 2024, 9, 29805−29819

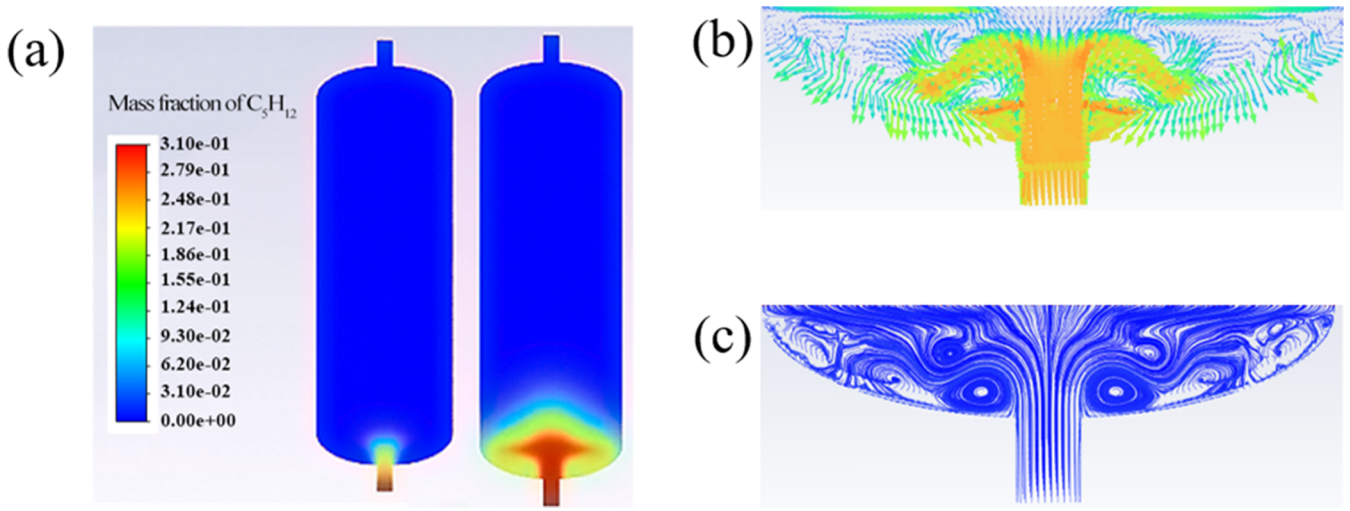

Figure 6. (a) Concentration distribution of gases to be adsorbed in the inlet section; (b) vector diagram of air velocity at the inlet head; (c) gas velocity traces at the inlet head.

v_j is the fractional velocity in the Y-axis direction, m/s

The viscous loss factor D_{ij} and the inertial loss factor C_{ij} are obtained by fitting velocity pressure drop curves for activated carbon. D_{ij} = 160,673,956 m^{-2}, C_{ij} = 10,018 m^{-1}.

2.4.3. Adsorption Kinetics Models. Accurate modeling of mass transfer kinetics is one of the necessary conditions to simulate dynamic adsorption processes. The adsorbed gas separation process, which is the transportation of gases from the bulk phase in the fixed bed to the interior of the adsorbent particles, includes both external and internal transport processes. The external transport process includes heat and mass transfer between the solid surface and the flowing fluid, called film diffusion. Internal transport processes include diffusion processes, in which gases penetrate into the porous structure. Under practical operating conditions, the total mass transfer rate is limited by pore diffusion, and the membrane diffusion resistance is negligible. The adsorption rate of oil and gas can be described by the linear driving force (LDF) model (set total resistance method) as shown in eqs 7 and 8. The LDF model is one of the most widely used models to simulate the adsorption process, which can express the mass transfer rate between gas−solid and solid phases very well. In this model, all mass transfer resistances are concentrated in one rate constant (MTC).

$$\frac{dq_i}{dt} = \mathrm{MTC}_i(q_i^* - q_i) \tag{7}$$

$$\frac{q_i}{q^*} = 1 - \exp(-\mathrm{MTC}_i^* t) \tag{8}$$

where

q_i^* is the adsorption capacity at equilibrium, mol/kg

q_i is the actual adsorption capacity at a given time t, mol/kg

MTC_i is the rate constant (1/s).

2.4.4. Thermodynamics of Adsorption. The equilibrium isotherm equation is one of the thermodynamic equations describing the adsorption of an adsorbent on an adsorbent. It is used to describe the variation of adsorption on the adsorbent with pressure at a certain temperature. It is very important for designing and optimizing the adsorption process.

The equilibrium isotherm equation is usually described by the Langmuir model or the Freundlich model. The Langmuir model assumes that monolayer adsorption is formed on the surface of the adsorbent, that only one molecule can be adsorbed at each adsorption site, and that the adsorption process is reversible. According to the Langmuir model, the equilibrium isotherm equation is given in eq 9.

$$q = kpq^*/(1 + kp) \tag{9}$$

where

q is the amount adsorbed, mol/kg

p is the equilibrium concentration in the gas phase, mol/kg

q^* is the maximum amount adsorbed, mol/kg

k is the adsorption equilibrium constant, a parameter describing the affinity of the adsorbent for the adsorbate.

2.4.5. Heat Balance Equation. The heat balance equation is fundamental in thermodynamics and energy systems. It expresses the principle of conservation of energy, stating that the total energy entering a system must equal the total energy leaving the system plus the change in energy stored within the system. Mathematically, it can be shown in eq 10.

$$Q_{in} - Q_{out} + W_{in} - W_{out} = \Delta U + \Delta K + \Delta P \tag{10}$$

where

Q_{in} is the heat added to the system

Q_{out} is the heat lost by the system

W_{in} is the work done on the system

W_{out} is the work performed by the system

ΔU is the change in the internal energy of the system

ΔK is the change in the kinetic energy of the system

ΔP is the change in the potential energy of the system.

2.5. High-to-Diameter Ratio. The determination of the H/D of the adsorption tank plays a crucial role in engineering design and contributes to the full utilization of the adsorbent. As can be seen from the concentration distribution of the gas to be adsorbed in the inlet section (Figure 6a), the gas velocity vector diagram at the inlet head (Figure 6b), and the trace diagram (Figure 6c), the gas enters the adsorption tank vertically with an uneven flow distribution and the inlet gas generates strong flows and large vortices along the elliptical head, the formation of these vortices leads to additional kinetic energy losses and to an increase in pressure drop. Although the gas is strongly diffusive and spreads rapidly at the head, it has a high resistance when it reaches the porous media zone and has to pass through a considerable thickness of the carbon layer to reach a

https://doi.org/10.1021/acsomega.4c03136
ACS Omega 2024, 9, 29805−29819

homogeneous state. The area between the saturated and nonadsorbed zones is called the adsorption zone. As the adsorption process proceeds, the adsorption zone gradually moves forward and the airflow into the adsorbent region is faster nearer the center, which leads to an earlier saturation of the adsorbent in the middle compared to the sides, resulting in an arc-shaped adsorption zone where the inlet surge leads to under-utilization of the adsorbent material in the inlet section. Therefore, this paper investigates the optimization of the tank height-to-diameter ratio and works to improve the utilization of the adsorbent.

The gas flow conditions of four different tanks with different height-to-diameter ratios are compared, penetration curves are obtained, and the optimum height-to-diameter ratio of the adsorption tank is selected through analysis and comparison. four adsorption tank sizes are shown in Table 2, and when changing the equipment height-to-diameter ratio, the volume of the porous media zone is kept constant and the ratio of the oil and gas inlet diameter to the diameter of the porous zone is kept constant. the controlled variable method is used to optimize the adsorption tank height-to-diameter ratio.

Table 2. Geometrical Parameters Used in the CFD of the Activated Carbon Layer

adsorption tank	tank I	tank II	tank III	tank IV
height (mm)	640	525	403	270
diameter (mm)	130	143	164	200
height-to-diameter ratio (H/D)	4.92	3.67	2.46	1.35
volume (cm^3)	8490.6			

2.6. Gas Distributors. Gas distributors play an important role in the operation of gas−solid and gas−liquid reactions and separation processes. In order to further improve the gas homogeneous state and increase the adsorbent utilization, a shell gas distributor is designed in the inlet zone with optimized structural parameters, such as pore distribution. The established 3D nozzle structure at the bottom of the industrial tower is shown in Figure 7. The gas is fed from the bottom and flows through three branches. Then, it is ejected through two rows of 99 small holes in the branches, with a 40° angle between the two rows of holes, one of which is oriented directly upward (22 holes). The other row of holes (11 holes) is 2.5 mm apart in the axial direction, with a circular, nonporous baffle of 80 mm diameter 18 mm from the top of the main flow path to reduce the gas velocity in the central area and avoid inlet surge.

Due to the complexity of the model, Fluent meshing is used for the 3D meshing. The workflow is chosen as a watertight workflow using the smooth-transition method. The mesh type is a high-fidelity tetrahedral mesh, a boundary layer is added to take into account the wall effect, which is closer to the real flow conditions of the fluid, and some small details such as small holes are locally encrypted. This is shown in Figure 8.

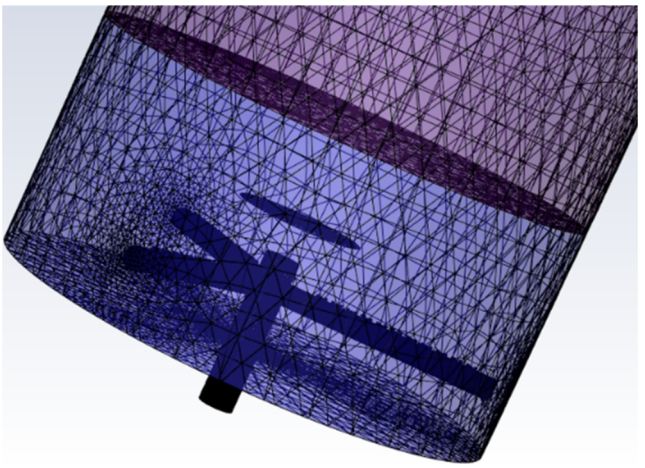

Figure 8. 3D meshing of the gas distributor.

The fluidization process is time-varying; therefore, transient simulations are chosen, taking into account the effect of gravity. The k-ε-RNG model is chosen for the viscosity model, which works well for strong streamline bending, swirling, and rotating flow models. Compared to the standard k-ε model, this model corrects for turbulent viscosity, takes into account the swirling flow situation, and can better handle flows with high strain rates and greater streamline curvature, more closely resembling realistic conditions. The use of the RNG/(k-ε) model modified for compressibility to simulate flow within a cavity avoids the distortions that occur with the standard k-ε model when simulating strong cyclonic flow or flow with curved walls and provides a higher degree of confidence and accuracy than the standard k-ε model. Therefore, the RNG/(k-ε) model is used to simulate the flow of the fluid inside the gas distributor. A suitable time step is chosen, gas is set as the ideal gas, and the boundary conditions are set as pressure inlet−pressure outlet with the outlet connected to the atmosphere to suppress back flow.

2.7. Pressure Swing Adsorption Process. Following completion of the computational fluid dynamics simulation to

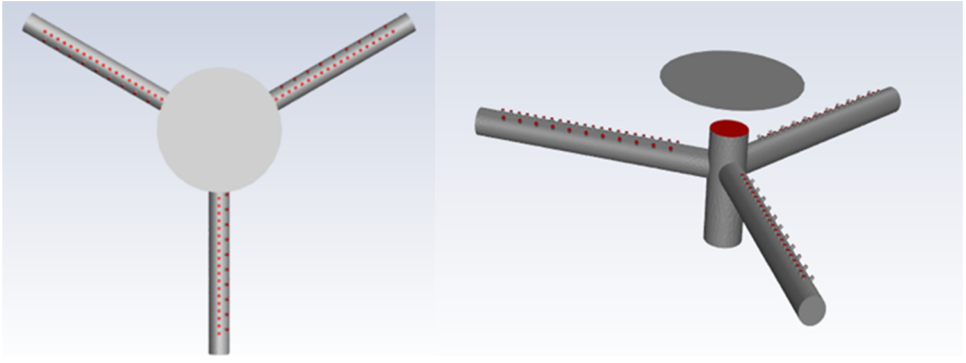

Figure 7. 3D structure of the gas distributor.

https://doi.org/10.1021/acsomega.4c03136
ACS Omega 2024, 9, 29805−29819

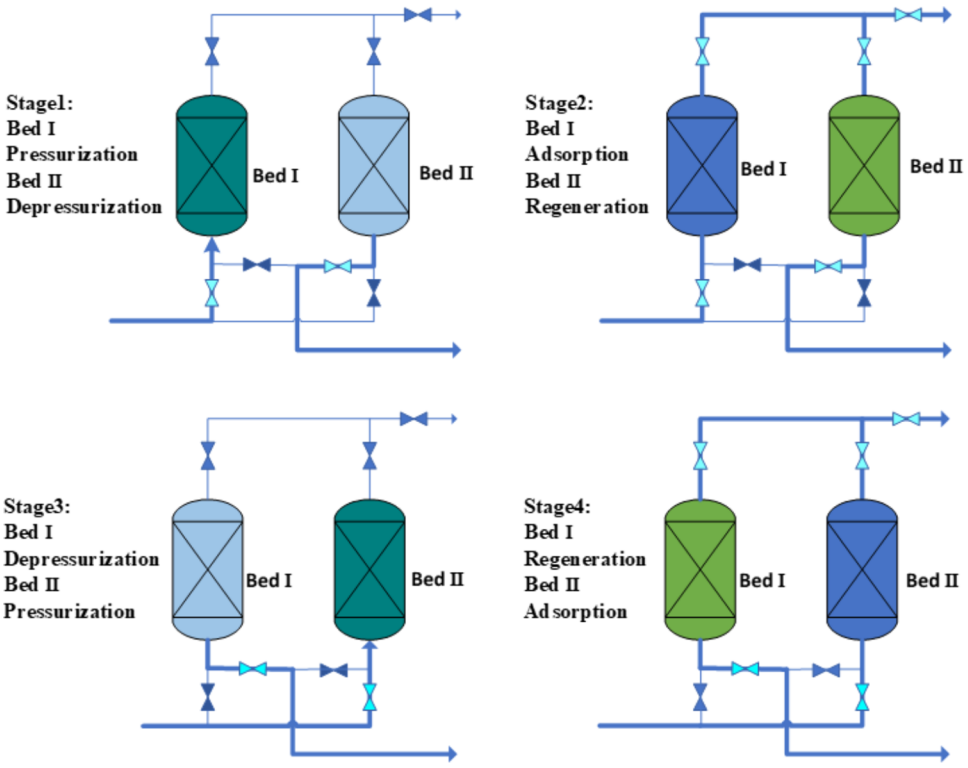

Figure 9. Four-step PSA process flow diagram.

Table 3. Adsorption Tower Basic Parameter Settings

parameter	numeric value	unit	remark
Hb	403	mm	adsorbent filling height
Db	164	mm	the inner diameter of the adsorption tower
E_i	0.5	(m^3void)/(m^3bed)	adsorption bed porosity
E_p	0.3	(m^3void)/(m^3bed)	adsorbent porosity
RHOs	610	kg/m^3	adsorbent bulk density
RP	4	mm	adsorbent particle size
SFac	1	n/a	spherical coefficient of sorbent particles

assess the flow field distribution within the adsorption tank, a more comprehensive investigation of the entire pressure swing adsorption process is conducted. This involved establishing a double-adsorption bed model and simulating the dynamic process of pressure swing adsorption process in four distinct steps as shown in Figure 9.[25,26] The aim is to optimize the operating parameters of the adsorption process from various perspectives. In the pressure swing adsorption process, the optimization variables include the adsorption pressure, feed flow rate, adsorption temperature, adsorption time, and purge ratio of the flushing step. Observed variables include purified air purity, recovery of desorbed oil and gas, and productivity. Based on the operating parameters and constraints of the above five optimizations, the dynamic cycle optimization of the PSA process of oil and gas is studied.

Suppose that two adsorption beds are initially filled with air under ambient conditions, under which the process is initialized and the simulation begins in dynamic operating mode. In dynamic mode, the penetration curve of the concentration of each component with time can be obtained, and the concentration change of oil gas and air produced at the outlet of the adsorption tank can be observed in real time. The dynamic simulation process of two-bed oil and gas PSA is divided into the following four steps: step groups 1 and 2 are collectively called the adsorption stage, and step groups 3 and 4 are collectively called the desorption and regeneration stage. The adsorption stage and the regeneration stage together constitute the oil and gas PSA process cycle.

- Step 1—Boost process: Open the feed valve, keep all other valves closed, and the high-pressure feed is boosted from the inlet end of the tower through the feed valve to prepare for the high-pressure adsorption process.
- Step 2—High-pressure adsorption: oil and gas are continuously passed into the adsorption bed at high pressure (3 bar). The oil and gas components are adsorbed in the activated carbon bed, forming a concentration wave to advance forward, the adsorbent gradually saturates along the gas flow direction, and the purified air flows out from the outlet end of the tower. When the concentration wave advances somewhere at the outlet end of the tower, the adsorption stops. Part of the purified air gas at the outlet of the adsorption tower is drawn out, and the other part is purged to tower II.
- Step 3—Pressure Relief Process: Open the extraction valve and keep all other valves closed to reduce the pressure to a lower level, this step is used to release the desorbed oil gas. Due to the pressure reduction, the

https://doi.org/10.1021/acsomega.4c03136
ACS Omega 2024, 9, 29805−29819

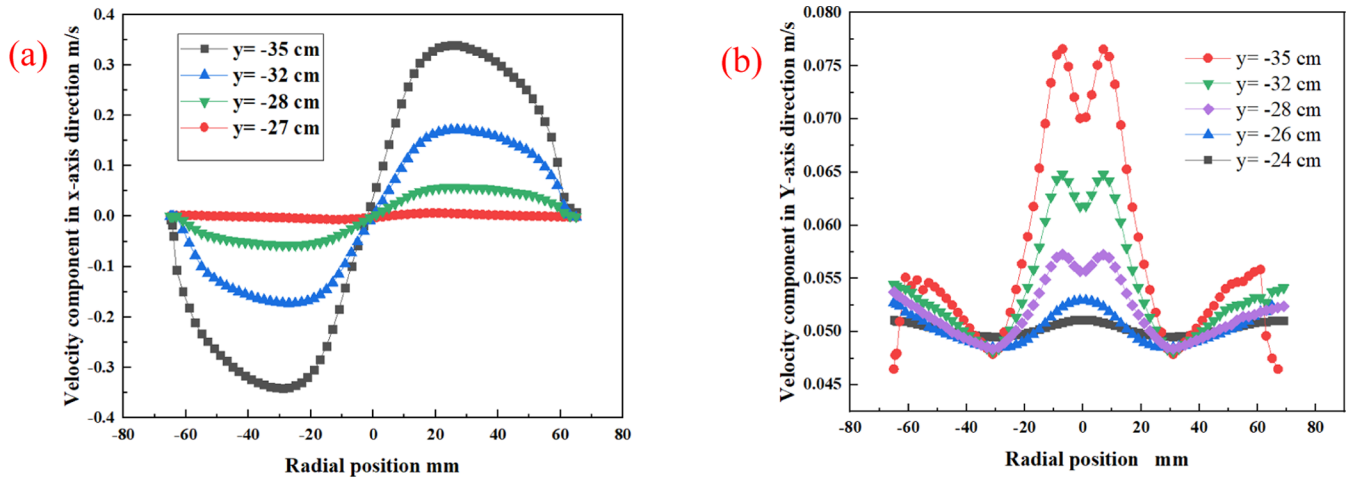

Figure 10. (a) Distribution of velocity components in the *x*-axis direction and (b) *Y*-axis direction.

adsorbed recombinant gas is desorbed, released from the inlet end of the adsorption tower through the extraction valve, and collected in the storage tank. While realizing the adsorbate desorption process, the saturated adsorbent is regenerated, and the concentration wave moves from the outlet end of the adsorption tower to the inlet end in this step.

- Step 4—Purge process: Column II is back-blown with a part of the gas flowing out of the top of tower I, this step is used to further reduce the partial pressure of the adsorbed in the bulk phase, promote the full desorption of the adsorbed components, diffuse to the gas-fluid phase by convection, and reverse purge the desorbed recombination components out of the adsorption tower by pumping out the valve, this process makes the adsorbent regeneration more complete and ready for the next cycle.

In the simulation setup of this paper, the adsorption bed is discretized into 40 nodes, which can effectively reduce the time complexity of the computational solution. The adsorption tower basic parameter settings are listed in Table 3.

The 4-step process flow of the oil and gas pressure swing adsorption process is established and optimized to comprehensively study the complete oil and gas PSA process. The structural parameters of the adsorption bed, i.e., the size of high Hb and diameter Db, are the result of optimizing the high diameter ratio of the adsorption tank. Since each state variable in the adsorption process is a function of time, it needs to be studied by dynamic simulation. The established double-tank adsorption model adopts the dynamic alternating mode of one suction and one removal. In the dynamic simulation process, the process cycle is constructed by the Cycle Organizer module to control the change of conditions, valve switching, flow change, etc., so that the pressure of the system changes periodically to realize the PSA process simulation. At the same time, considering the five factors affecting the efficiency of oil and gas adsorption, the operating parameters and operating conditions of the pressure swing adsorption process are comprehensively studied to reveal the influence of each operating parameter and operating conditions on the PSA process more comprehensively.

3. RESULTS AND DISCUSSION

3.1. Velocity Distribution. Figure 10a,b shows the distribution of the radial and axial components of the velocity at different radial positions for H/D = 2.46. It can be seen from the figures that the gas enters the fixed bed adsorption tank vertically with an uneven flow distribution. With increasing H/D, the variation in flow rate inside the fixed bed slows down and the gas is more uniformly distributed. The geometry of the adsorption bed of the four tanks in the CFD simulation is shown in Table 4, keeping the volume of the adsorbent constant when changing the bed height-to-diameter ratio.

Table 4. Carbon Layer Thickness Required for a Uniform Velocity Distribution

adsorption tank	tank I	tank II	tank III	tank IV
H/D	4.92	3.67	2.46	1.35
In *X*-axis direction (mm)	24	38	50	64
In *Y*-axis direction (mm)	56	73	90	118

Table 4 shows the thickness of the activated carbon layer that needs to be crossed for the velocity to reach homogeneity in the four different height-to-diameter ratios of the tanks. As can be seen from Table 4, the smaller the height-to-diameter ratio, i.e., the slimmer the tank, the more uneven the flow distribution. As the high diameter ratio continues to increase, the internal flow rate of the fixed bed changes more insignificantly and is more evenly distributed. The flow uniformity can indirectly reflect the utilization rate of the adsorbent and the adsorption performance of the adsorbent.

3.2. Penetration Curves. Figure 11a shows the sorption penetration curves for C_4H_{10} at different H/D (up to the GB31571-2015 emission standard, which is 20 mg/m^3 in this study). It can be observed in the graph that the penetration time increases monotonically from 39 to 92 min as the H/D increases from 1.35 to 4.92. It can also be observed that the activated carbon bed is completely penetrated at almost the same time (approximately 118 min) for different H/D conditions, i.e., the easily adsorbed components of the oil and gas are no longer adsorbed but only pass through the adsorbent bed. However, although their penetration times are almost identical, the total amount of C_4H_{10} adsorbed differs for the different H/D carbon layers, the higher the H/D of the adsorbent bed, the greater the amount of C_4H_{10} adsorbed. The reason for this can be explained by the fact that for a given amount of adsorbent and gas volume flow rate, the higher gas flow rate due to the narrower diameter of the adsorbent bed with higher H/D leads to a higher Reynolds

https://doi.org/10.1021/acsomega.4c03136
ACS Omega 2024, 9, 29805−29819

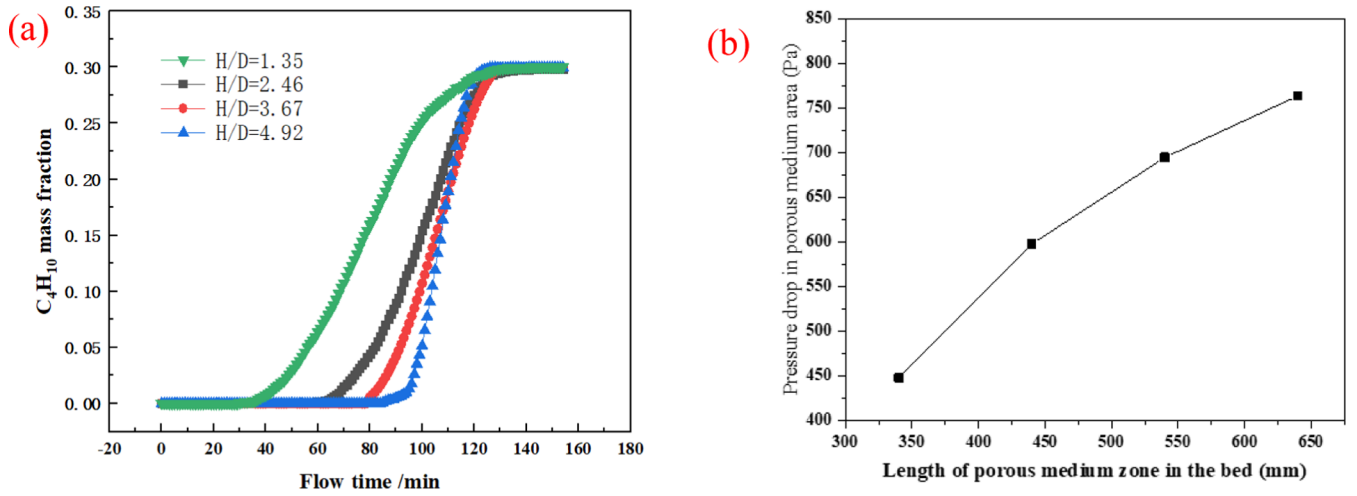

Figure 11. (a) Penetration curves for different height-to-diameter ratios; (b) pressure drop−porous media zone length correlation.

number ($Re = du\rho/\mu$), indicating that stronger turbulence occurs in the bed. This turbulence allows for an enhanced mass transfer of oil and gas from the bulk phase to the interior of the activated carbon. On the other hand, "pseudo-channels" may be formed in the bed, through which the gas stream passes without adsorption occurring. It can be inferred that the higher the H/D ratio of the bed, the less "pseudo-channels" are formed.

However, as the height-to-diameter ratio increases, the pressure drops generated increase, which can pose a safety hazard, as shown in Figure 11b, where the pressure drop increases as the porous media zone becomes longer. However, the axial pressure gradient due to increased bed flow resistance is not conducive to regeneration of the adsorbent, which can result in higher energy costs. The net effect of the pressure drop is to increase the purity of the light product and reduce the recovery rate for the same throughput. In practice, this will inevitably lead to a loss of purity as a large amount of recombination is allowed to leave the bed during the production step, thereby contaminating the collected pure product. The pressure drop also means higher energy costs and more mechanical problems in the adsorbent and adsorber design. Therefore, in order to increase the mechanical strength of the adsorber tower, additional capital investment in equipment is required.

3.3. Gas Distributor. The CFD simulation results of the inlet gas distributor are postprocessed; that is, the CFD solver results data are visualized to obtain the distributor pressure distribution cloud (a), and the velocity distribution vector diagram (b) in Figure 12. The results of the velocity distribution cloud and vector diagram of the fluid show that the gas enters from the vertical main flow path at high pressure and then exits from two rows of small holes in the three bypasses. According to the simulation results of the velocity distribution cloud and vector diagrams in Figure 12, the gas is ejected from the small holes and, due to the high diffusivity of the gas, is already diffused uniformly before it reaches the porous adsorption zone. The gas distribution state at the entrance to the porous zone of interest is, therefore, uniformly distributed.

It can be seen from Figure 13 that the addition of the inlet gas distributor increases the penetration time in the penetration curve by 8.7 min, and the diffusion is more uniform. This means that it increases the time for the adsorbent to reach the penetration state and improves the adsorbent utilization. In addition, the designed distributor is also suitable for larger diameter towers. It can reasonably predict the gas holdup

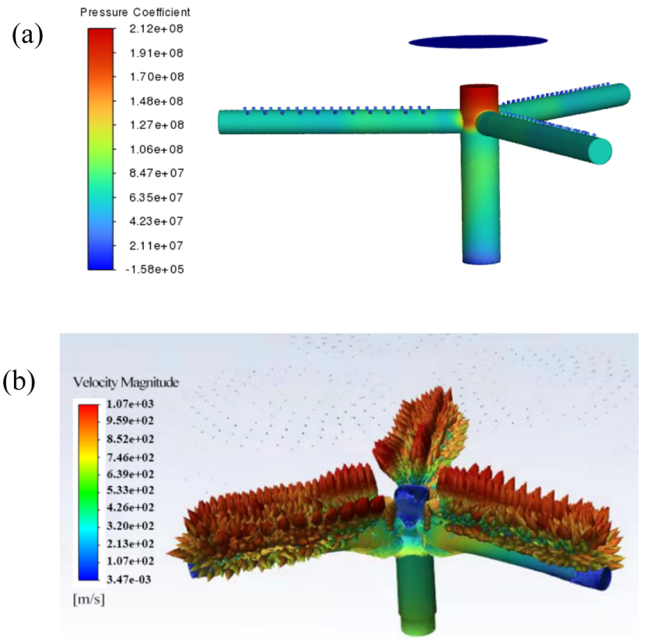

Figure 12. Gas distributor distributer pressure distribution cloud (a). Velocity distribution vector diagram (b).

distribution at different apparent gas velocities and improve the gas predistribution performance in many types of packed particle beds.

3.4. PSA Optimization of Operating Parameters. *3.4.1. Optimized Adsorption Time.* The adsorption time greatly affects the pressure swing adsorption performance, and the prediction of adsorption penetration time can be determined using the penetration curve.[27,28] Figure 14a is a schematic of the penetration curve, which depicts the adsorbate concentration in the effluent of the adsorption tank, m.

Due to the presence of multiple components in oil and gas, the affinity between each component and the adsorbent is different, and when the adsorption capacity reaches the maximum load of the bed, a competitive adsorption process occurs between the components. The components adsorbed on the surface of the adsorbent are displaced; that is, the components with lower affinity with the adsorbent are replaced by other components with higher affinity, desorbed from the adsorbent, and rereleased

https://doi.org/10.1021/acsomega.4c03136
ACS Omega 2024, 9, 29805−29819

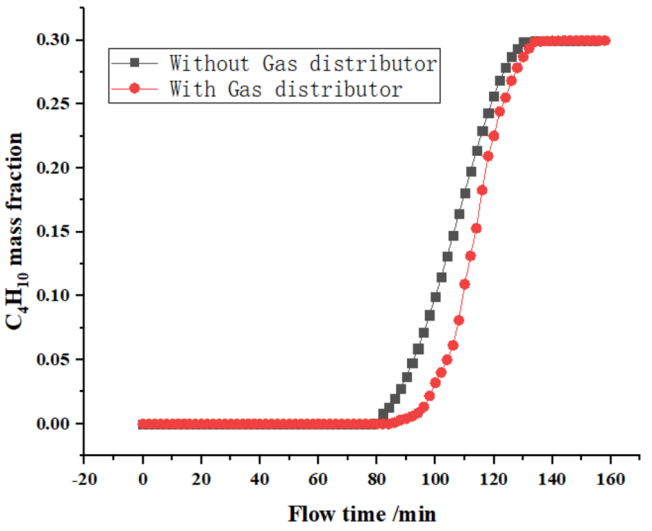

Figure 13. Comparison of penetration curves with and without the gas distributor.

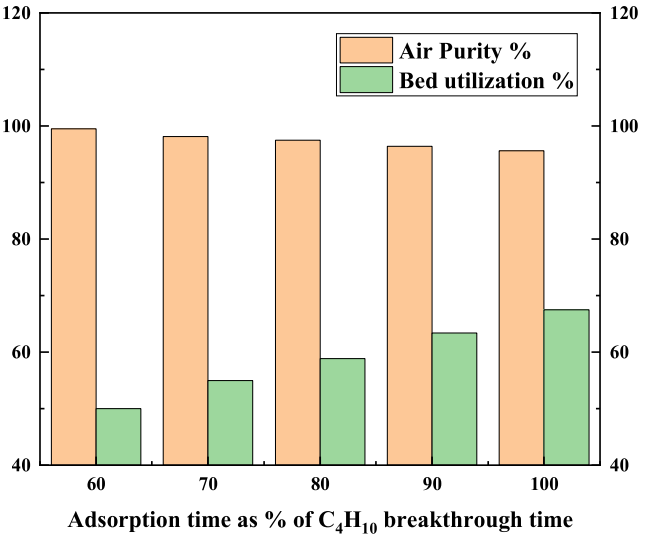

Figure 15. Effect of different adsorption times on air purity and activated carbon bed utilization.

into the bulk phase. Due to the existence of a competitive adsorption phenomenon, the C_4H_{10} component, which is relatively low with activated carbon, will penetrate first, so the penetration time of the C_4H_{10} component is used as the time when the penetration phenomenon of oil and gas occurs. The adsorption time is set to 60∼100% of the C_4H_{10} penetration time (BT), and the effect of the running time of the adsorption step on the purified air purity and the utilization rate of the adsorbent are compared. With the operation of the adsorption process, a certain concentration of adsorbate will accumulate on the surface of the adsorbent, which is called the adsorption load, and the utilization of the adsorption bed can be obtained according to the distribution of the adsorption load of the bed.

Figure 15 shows the effects of different adsorption times on air purity and utilization rate of the activated carbon bed. When the adsorption step size of the PSA cycle is set to 60% of the C_4H_{10} penetration time, the average purity of the purified air can reach 99.5 mol %. The bed utilization rate is about 50%. When the adsorption time increases to 70% of the C_4H_{10} penetration time, the purity drops to 98.2 mol %, but the bed utilization increases to about 55%. With the increase of adsorption time, the purity value of the purified air further decreases and the utilization rate of the bed continues to increase. At 100% of the adsorption time of C_4H_{10} penetration time, the average purity of the purified air is 95.6 mol, and the bed utilization increases to about 67.5%. In this study, the adsorption step is set to 70% of the C_4H_{10} penetration time due to the need to ensure the purity of the purified air and to make the bed utilization as high as possible.

The above conclusion can be explained by the following facts: with the increase in the adsorption step time, the oil and gas mass transfer front gradually moves to the outlet end of the adsorption tank, which leads to partial leakage of oil and gas from the tower and reduces the air purity. At the same time, due to the continuous advancement of the mass transfer area, the activated carbon area that is not fully utilized at the outlet end decreases, which improves the utilization rate of the adsorbent.

3.4.2. Optimized Adsorption Pressure. The influence of adsorbents on air purification and oil and gas purification performance is mainly evaluated by air purity, oil and gas recovery, and productivity. It can be seen from Figure 16 that with the gradual increase of the adsorption operation pressure, the amount of gas processed by the adsorbent increases under the same operating conditions as other operating conditions. This is because the physical adsorption process is caused by van der Waals force; with the increase of operating pressure, the

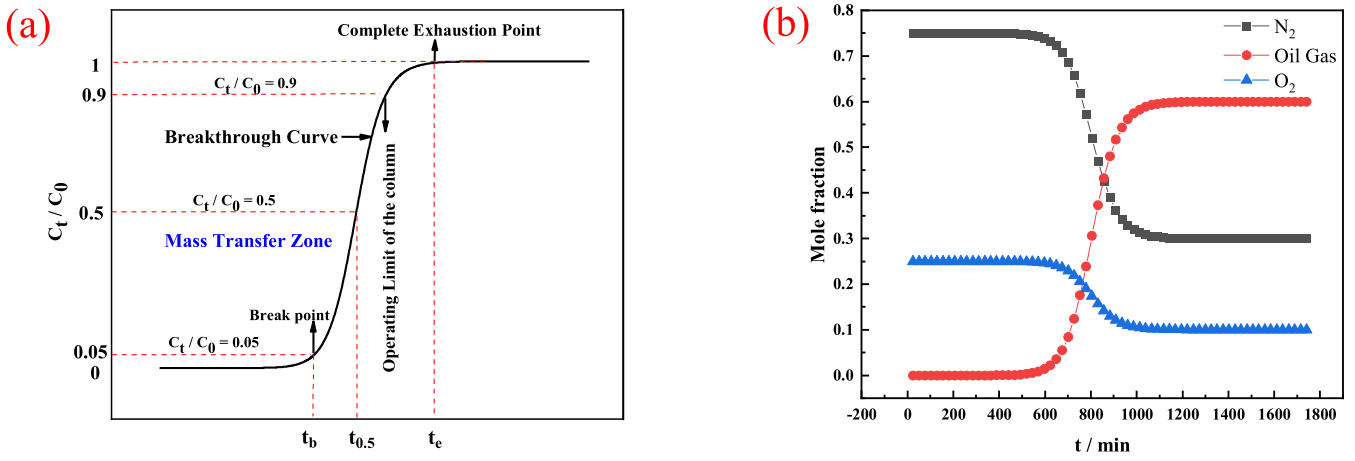

Figure 14. (a) Schematic diagram of penetration curve. (b) Oil and gas penetration curve.

https://doi.org/10.1021/acsomega.4c03136
ACS Omega 2024, 9, 29805−29819

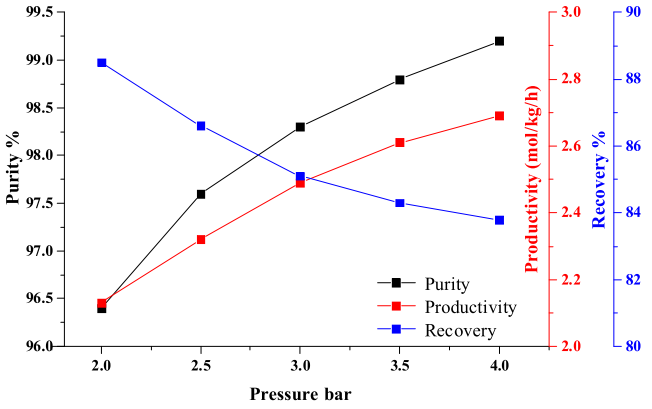

Figure 16. Correlation diagram of the pressure−adsorption and desorption performance.

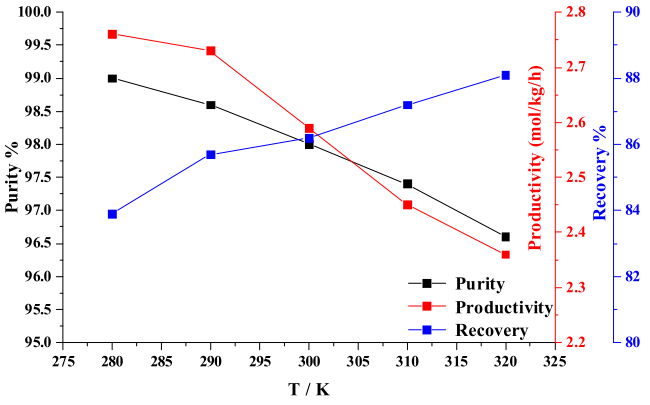

Figure 18. Correlation diagram of the temperature−adsorption and desorption performance.

interaction force between the adsorbent and the adsorbate increases, the mass transfer driving force increases, and the adsorption bed can adsorb more gases to be adsorbed in the same adsorption time, thereby improving the purity of air and the productivity of oil and gas. At the same time, during the pressurization phase, the recovery rate of oil and gas will be reduced accordingly, as more gas is introduced into the adsorption bed. Since more attention is paid to the purified air purity and oil vapor recovery in this study, 3 bar is chosen as the operating pressure for the adsorption process.

3.4.3. Temperature Optimization. As shown in Figure 17, the effect of pressure on adsorption performance shows the

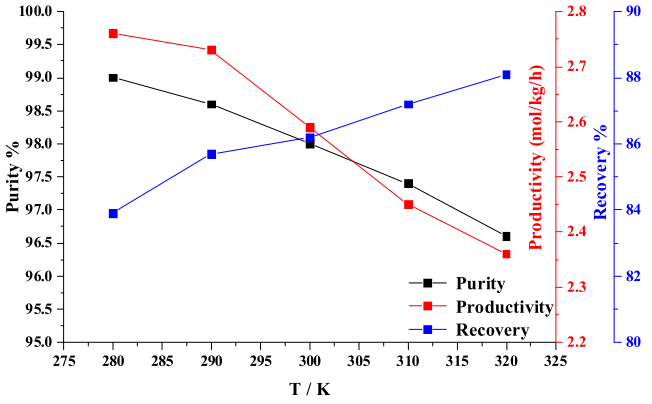

Figure 17. Correlation diagram of temperature−adsorption and desorption performance.

opposite trend; the higher the temperature, the less the adsorption capacity, resulting in the purity of air and the productivity of oil and gas decreasing with increasing temperature. Therefore, high temperature is not conducive to the oil and gas adsorption process. However, the corresponding desorption performance is enhanced, the desorption is relatively complete, less gas remains in the adsorbent, and the adsorbent regeneration effect becomes better. Under the premise of ensuring the air purification effect, it is hoped that the higher the recovery rate and yield of oil and gas, the better, so the operating temperature is selected to be 290 K.

3.4.4. Optimized Air Velocity of the Empty Tower. It can be seen from Figure 18 that when other simulation conditions are fixed, within a certain range, the gas velocity of the air tower has a greater impact on the performance of the adsorption process; with the increase of the air tower gas velocity, the residence time of the adsorbate in the bed becomes shorter, and the more adsorbate treated with the same amount of adsorbent in the same time, the greater the adsorption load. Air purity increases, oil and gas recovery decreases, and yield increases. However, after the gas velocity exceeds a certain range, the amount of gas passing through the bed per unit time increases, resulting in a decrease in air purity and an increase in oil and gas recovery. Therefore, the air velocity of the empty tower is selected to be 0.45 m/s. From the results of the adsorption performance, it can be seen that air purity and oil and gas recovery rate show the opposite trend.

3.4.5. Purge Ratio Optimization. This step aims to regenerate the adsorbent by adjusting the purge gas flow to desorb the adsorbent material from the adsorbent surface.[29] A certain amount of adsorbate will remain in the adsorbent in the adsorbent in the adsorption tower, and if regeneration treatment is not carried out, the adsorption capacity of the adsorption tower will be reduced. During the purging process, by reducing the partial pressure of the purge gas, the adsorbate molecules will be desorbed from the surface of the adsorbent and discharged from the adsorption tower with the purge gas so that the adsorbent returns to the original adsorption state. The end condition of this step is judged according to the fraction of the light component in the outflow gas, and the purge process can be ended when the fraction of the light component in the outflow gas is greater than a certain value (0.8). As P/F increases, air purity, oil and gas recovery, and yield all increase. This is because the partial pressure of the adsorbate in the bulk phase is greatly reduced in the procedure of purging the bed with air, making it easier to desorb from the adsorption bed. This step allows for more complete sorbent regeneration, resulting in improved oil and gas recovery and yield. A sharper mass transfer front is created in the next circulating adsorption step, increasing the purity of the air purification. However, at the same time, it should be noted that because this step needs to be purged with product gas, which will reduce the output of product gas, it should be selected according to the actual needs of the industry. In the oil and gas treatment process, it aims to reduce the pollution caused by oil and gas emissions into the atmosphere, and at the same time for the recovery and utilization of oil and gas resources. It can be seen from Figure 19 that there is no objective demand for air production, so a larger purge ratio can be selected. Therefore, P/F is chosen as 0.3.

https://doi.org/10.1021/acsomega.4c03136
ACS Omega 2024, 9, 29805−29819

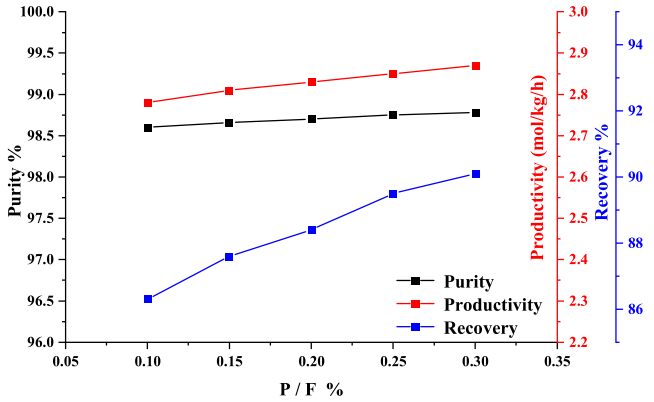

Figure 19. Correlation diagram of purge ratio−adsorption and desorption performance.

4. CONCLUSIONS

The discussion in this work allows us to draw the following conclusions. In the equipment strengthening stage, the size of the adsorption tank with a height/diameter ratio of k = 2.46 is selected as the input structural parameter for the adsorption bed layer, with a height Hb of 403 mm and a diameter Db of 164 mm. The designed inlet gas distributor has a good effect and can effectively reduce the large eddy currents at the inlet of porous media and the high gas velocity on the axis. This increases the penetration time in the penetration curve by 8.7 min, which means it increases the time for the adsorbent to reach the penetration state and improves the utilization rate of the adsorbent. In the simulation and optimization part of the oil and gas pressure swing adsorption process, a recyclable dual tank adsorption model is established, taking into account five factors that affect the efficiency of oil and gas adsorption. A comprehensive study is conducted of the operating parameters of the pressure swing adsorption process. The optimized operating parameters are: adsorption time of 70% of C_4H_{10} penetration time, adsorption pressure of 3 bar, adsorption temperature of 290 K, empty tower gas velocity of 0.45 m/s, and blowing ratio of 0.3. These parameters make the adsorption performance of the activated carbon adsorbent optimal.

AUTHOR INFORMATION

Corresponding Author

Wende Tian − *College of Chemical Engineering, Qingdao University of Science & Technology, Qingdao 266042, P. R. China;* orcid.org/0000-0002-8270-8947; Phone: +86-532-84022750; Email: tianwd@qust.edu.cn

Authors

Bin Liu − *College of Chemical Engineering, Qingdao University of Science & Technology, Qingdao 266042, P. R. China*

Mengjiao Zhang − *College of Chemical Engineering, Qingdao University of Science & Technology, Qingdao 266042, P. R. China;* orcid.org/0009-0009-4239-6959

Ye Tao − *College of Chemical Engineering, Qingdao University of Science & Technology, Qingdao 266042, P. R. China*

Zhe Cui − *College of Chemical Engineering, Qingdao University of Science & Technology, Qingdao 266042, P. R. China;* orcid.org/0000-0002-0765-8863

Complete contact information is available at: https://pubs.acs.org/10.1021/acsomega.4c03136

Notes

The authors declare no competing financial interest.

ACKNOWLEDGMENTS

The authors gratefully acknowledge that this work was supported by the Youth Project of Shandong Provincial Natural Science Foundation (grant no. ZR2022QB174), the National Natural Science Foundation of China (grant no. 22178189), the National Natural Science Foundation of China (grant no. 22308184), the Shandong Natural Science Foundation (grant no. ZR2021MB113), and the Shandong Natural Science Foundation (grant no. ZR2022QB020).

REFERENCES

(1) He, C.; Cheng, J.; Zhang, X.; Douthwaite, M.; Pattisson, S.; Hao, Z. Recent Advances in the Catalytic Oxidation of Volatile Organic Compounds: A Review Based on Pollutant Sorts and Sources. *Chem. Rev.* **2019**, *119*, 4471−4568.

(2) Huang, Y.; Ho, S. S. H.; Lu, Y.; Niu, R.; Xu, L.; Cao, J.; Lee, S. Removal of Indoor Volatile Organic Compounds via Photocatalytic Oxidation: A Short Review and Prospect. *Molecules* **2016**, *21*, 56.

(3) Krishnamurthy, A.; Adebayo, B.; Gelles, T.; Rownaghi, A.; Rezaei, F. Abatement of gaseous volatile organic compounds: A process perspective. *Catal. Today* **2020**, *350*, 100−119.

(4) Kamal, M. S.; Razzak, S. A.; Hossain, M. M. Catalytic oxidation of volatile organic compounds (VOCs) - A review. *Atmos. Environ.* **2016**, *140*, 117−134.

(5) Dwivedi, P.; Gaur, V.; Sharma, A.; Verma, N. Comparative study of removal of volatile organic compounds by cryogenic condensation and adsorption by activated carbon fiber. *Sep. Purif. Technol.* **2004**, *39*, 23−37.

(6) Yang, C.; Miao, G.; Pi, Y.; Xia, Q.; Wu, J.; Li, Z.; Xiao, J. Abatement of various types of VOCs by adsorption/catalytic oxidation: A review. *Chem. Eng. J.* **2019**, *370*, 1128−1153.

(7) Li, X.; Zhang, L.; Yang, Z.; Wang, P.; Yan, Y.; Ran, J. Adsorption materials for volatile organic compounds (VOCs) and the key factors for VOCs adsorption process: A review. *Sep. Purif. Technol.* **2020**, *235*, No. 116213.

(8) Zheng, M.; Hu, H.; Zhang, G.; Ye, Z.; Chen, X. Combination of adsorption-diffusion model with CFD for study of desulfurization in fixed bed. *J. Environ. Chem. Eng.* **2017**, *5*, 4141−4150.

(9) Di Carlo, A.; Aloisi, I.; Jand, N.; Stendardo, S.; Foscolo, P. U. Sorption enhanced steam methane reforming on catalyst-sorbent bifunctional particles: A CFD fluidized bed reactor model. *Chem. Eng. Sci.* **2017**, *173*, 428−442.

(10) Chen, C.; Guan, X.; Ren, Y.; Yang, N.; Li, J.; Kunkelmann, C.; et al. Mesoscale modeling of emulsification in rotor-stator devices: Part I: A population balance model based on EMMS concept. *Chem. Eng. Sci.* **2019**, *193*, 171−183.

(11) Salim Bded, A. Performance Simulation for Gas Flow through a Porous Media in Packed bed Columns using CFD. *IOP Conf. Ser.: Mater. Sci. Eng.* **2019**, *579*, No. 012001.

(12) Bai, X.; Isaac, K.; Klein, D.; Banerjee, R.; Edson, J.; Breig, W. F.et al. Multidimensional, Time-Accurate CFD Simulation of Adsorption/Desorption in a Carbon Canister. 2003-01-1003. DOI: 10.1088/1757-899X/579/1/012001.

(13) Montecchio, F.; Babler, M. U.; Engvall, K. Development of an irradiation and kinetic model for UV processes in volatile organic compounds abatement applications. *Chem. Eng. J.* **2018**, *348*, 569−582.

(14) Nouh, S. A.; Lau, K. K.; Shariff, A. M. Modeling and simulation of fixed bed adsorption column using integrated CFD approach. *J. Appl. Sci.* **2010**, *10*, 3229−3235.

(15) Hou, X.; Liu, X.; Liu, Z.; Yan, F.; Yuan, S.; Jin, X. *Flow Field Simulation and Experimental Evaluation of Carbon Canister based on FLUENT*, 2010 International Conference on Computational Intelligence and Software Engineering, CiSE 2010; IEEE Computer Society, 2010. DOI: 10.1109/CISE.2010.5677143.

(16) Fangueiro Gomes, L.; Augier, F.; Leinekugel-le-Cocq, D.; Vinkovic, I.; Simoens, S. Hydrodynamic modelling of complex fixed bed geometries in simulated moving bed adsorption processes. *Chem. Eng. Sci.* **2015**, *132*, 46−58.
(17) Hou, Y.; Gong, Y.; Zhu, L.; Chen, J. Experimental and Numerical Simulation Study on Process Parameters of Activated Carbon Adsorption of Benzene. *Ind. Saf. Environ. Prot.* **2017**, *43*, 76−79+88.
(18) Buzanowski, M. A.; Yang, R. T.; Haas, O. W. Direct observation of the effects of bed pressure drop on adsorption and desorption dynamics. *Chem. Eng. Sci.* **1989**, *44*, 2392−2394.
(19) Darakchiev, R.; Dodev, C. Gas flow distribution in packed columns. *Chem. Eng. Process.* **2002**, *41*, 385−393.
(20) Waldron, W. E.; Sircar, S. Parametric study of a pressure swing adsorption process. *Adsorption* **2000**, *6*, 179−188.
(21) Hosseini, S. M.; Alizadeh, R.; Alizadehdakhel, A.; Behjat, Y.; Nooriasl, P. Enhancement of gas distribution uniformity in a claus process catalytic reactor using computational fluid dynamics. *Chem. Eng. Process.* **2019**, *144*, No. 107653.
(22) Li, L.; Lian, W.; Bai, B.; Zhao, Y.; Li, P.; Zhang, Q.; et al. CFD-PBM investigation of the hydrodynamics in a slurry bubble column reactor with a circular gas distributor and heat exchanger tube. *Chem. Eng. Sci.: X* **2021**, *9*, No. 100087.
(23) Wang, S.; Sun, X.; Xu, C.; Bao, J.; Peng, C.; Tang, Z. Investigation of a circulating turbulent fluidized bed with a fractal gas distributor by electrostatic-immune electrical capacitance tomography. *Powder Technol.* **2020**, *361*, 562−570.
(24) Liu, B.; Xiao, Q.; Sun, N.; Gao, P.; Fan, F.; Sunden, B. Effect of gas distributor on gas−liquid dispersion and mass transfer characteristics in stirred tank. *Chem. Eng. Res. Des.* **2019**, *145*, 314−322.
(25) Law, L. C.; Abdullah, A.; Idris, I.; Othman, M. R. Effect of pressure equalization on methane enrichment from stranded natural gas using PSA with amorphous Kenaf and microporous palm kernel shell adsorbents. *Int. J. Energy Res.* **2020**, *44*, 6555−6566.
(26) Santos, M. P. S.; Grande, C. A.; Rodrigues, A. E. Pressure Swing Adsorption for Biogas Upgrading. Effect of Recycling Streams in Pressure Swing Adsorption Design. *Ind. Eng. Chem. Res.* **2011**, *50* (2), 974−985.
(27) Escudero, C.; Poch, J.; Villaescusa, I. Modelling of breakthrough curves of single and binary mixtures of Cu(II), Cd(II), Ni(II) and Pb(II) sorption onto grape stalks waste. *Chem. Eng. J.* **2013**, *217*, 129−138.
(28) Balanay, J. A. G.; Oh, J. Adsorption Characteristics of Activated Carbon Fibers in Respirator Cartridges for Toluene. *Int. J. Environ. Res. Public Health* **2021**, *18*, 8505.
(29) De Witte, N.; Denayer, J. F. M.; Van Assche, T. R. C. Effect of Adsorption Duration and Purge Flowrate on Pressure Swing Adsorption Performance. *Ind. Eng. Chem. Res.* **2021**, *60*, 13684−13691.

https://doi.org/10.1021/acsomega.4c03136
ACS Omega 2024, 9, 29805−29819